Title

Autistic-like behavior, spontaneous seizures, and increased neuronal excitability in a Scn8a mouse model

Journal

Neuropsychopharmacology, 46(11)

ISSN

0893-133X

Authors

Wong, Jennifer C
Grieco, Steven F
Dutt, Karoni
et al.

Publication Date

2021-10-01

DOI

10.1038/s41386-021-00985-9

Neuropsychopharmacology

www.nature.com/npp

ARTICLE

Autistic-like behavior, spontaneous seizures, and increased neuronal excitability in a *Scn8a* mouse model

Jennifer C. Wong[1], Steven F. Grieco[2], Karoni Dutt[3], Lujia Chen[2], Jacquelyn T. Thelin[1], George Andrew S. Inglis[1], Shangrila Parvin[4], Sandra M. Garraway[4], Xiangmin Xu[2], Alan L. Goldin[3] and Andrew Escayg[1]

Patients with *SCN8A* epileptic encephalopathy exhibit a range of clinical features, including multiple seizure types, movement disorders, and behavioral abnormalities, such as developmental delay, mild-to-severe intellectual disability, and autism. Recently, the de novo heterozygous *SCN8A* R1620L mutation was identified in an individual with autism, intellectual disability, and behavioral seizures without accompanying electrographic seizure activity. To date, the effects of *SCN8A* mutations that are primarily associated with behavioral abnormalities have not been studied in a mouse model. To better understand the phenotypic and functional consequences of the R1620L mutation, we used CRISPR/Cas9 technology to generate mice expressing the corresponding *SCN8A* amino acid substitution. Homozygous mutants exhibit tremors and a maximum lifespan of 22 days, while heterozygous mutants (RL/+) exhibit autistic-like behaviors, such as hyperactivity and learning and social deficits, increased seizure susceptibility, and spontaneous seizures. Current clamp analyses revealed a reduced threshold for firing action potentials in heterozygous CA3 pyramidal neurons and reduced firing frequency, suggesting that the R1620L mutation has both gain- and loss-of-function effects. In vivo calcium imaging using miniscopes in freely moving RL/+ mutants showed hyperexcitability of cortical excitatory neurons that is likely to increase seizure susceptibility. Finally, we found that oxcarbazepine and Huperzine A, a sodium channel blocker and reversible acetylcholinesterase inhibitor, respectively, were capable of conferring robust protection against induced seizures in RL/+ mutants. This mouse line will provide the opportunity to better understand the range of clinical phenotypes associated with *SCN8A* mutations and to develop new therapeutic approaches.

Neuropsychopharmacology (2021) 46:2011–2020; https://doi.org/10.1038/s41386-021-00985-9

INTRODUCTION

SCN8A, encoding the voltage-gated sodium channel $Na_v1.6$, is expressed in both excitatory and inhibitory neurons, and $Na_v1.6$ channels are highly concentrated in axon initial segments and nodes of Ranvier [1–3]. Furthermore, $Na_v1.6$ is a critical mediator of neuronal excitability, playing an important role in the initiation and propagation of action potentials (APs) [4]. Persistent and resurgent currents have also been shown to be mediated by $Na_v1.6$ [5, 6].

We previously demonstrated that mice with heterozygous loss-of-function *Scn8a* mutations, or alleles with reduced activity, exhibit increased resistance to electrically and chemically induced seizures [7–9], and that the coexpression of such alleles in mouse models of *SCN1A*-derived epilepsy can ameliorate seizure phenotypes and increase lifespan [7, 8]. We also demonstrated that selective reduction of *Scn8a* expression in the hippocampus is sufficient to prevent the development of spontaneous seizures and ameliorate hyperactive behavior in a mouse model of mesial temporal lobe epilepsy [10]. However, depending on the genetic background, spike-wave discharges, a hallmark of absence epilepsy, have been observed in mice with loss-of-function *Scn8a* alleles [11]. Recently, reduced *Scn8a* expression in the reticular thalamic nucleus was shown to lead to disruption in cell intrinsic excitability and impaired synaptic inhibition, resulting in spike-wave discharges [12].

The first human *SCN8A* epilepsy-associated mutation, N1768D, was reported in 2012 [13], and since then over 200 primarily de novo missense mutations have been identified [14, 15] accounting for ~1% of epileptic encephalopathy cases (https://ghr.nlm.nih.gov [16]). More recently, the N1768D mutation was knocked into the mouse *Scn8a* gene ($Scn8a^{N1768D}$), providing the first *Scn8a* mouse model of epileptic encephalopathy [17]. Heterozygous mutant mice recapitulated many of the clinical features observed in the $SCN8A^{N1768D}$ proband, including spontaneous seizures, interictal spiking, and sudden unexpected death in epilepsy (SUDEP) [17]. Behavioral analysis of these mutant mice also revealed normal sociability but deficits in social discrimination[17]. A subset of the de novo missense mutations in *SCN8A* are recurrent, including R850Q and R1872W [14]. Recently, a conditional mouse with knock-in of the *SCN8A* R1872W mutation was generated, and it was shown that expression of this mutation in forebrain excitatory neurons was sufficient to cause premature lethality and spontaneous seizures [18]. Behavioral analysis was not conducted in the conditional R1872W mutants.

Patients with *SCN8A* mutations present with a spectrum of clinical features, including multiple seizure types, movement disorders, and behavioral abnormalities, such as developmental delay, mild-to-severe intellectual disability, and autism [15, 19]. Using a diagnostic exome sequencing approach in individuals

[1]Department of Human Genetics, Emory University, Atlanta, GA, USA; [2]Department of Anatomy and Neurobiology, University of California Irvine, Irvine, CA, USA; [3]Department of Microbiology and Molecular Genetics, University of California Irvine, Irvine, CA, USA and [4]Department of Physiology, Emory University, Atlanta, GA, USA
Correspondence: Jennifer C. Wong (jennifer.c.wong@emory.edu)

Received: 13 March 2020 Revised: 1 February 2021 Accepted: 2 February 2021
Published online: 3 March 2021

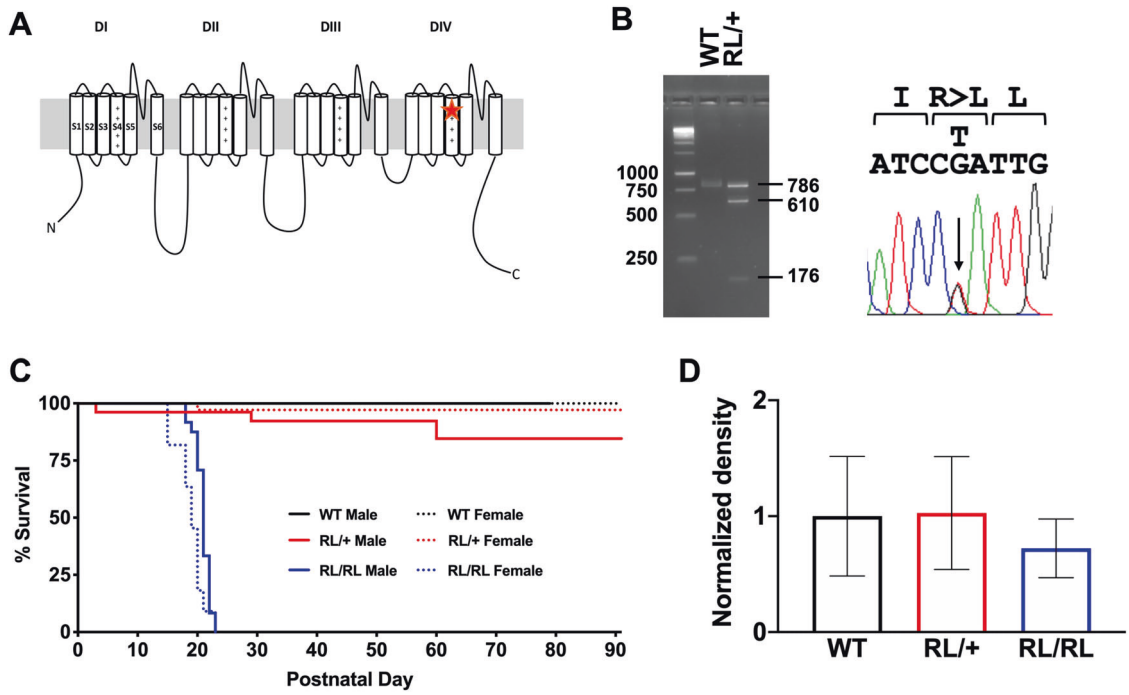

Fig. 1 Generation and characterization of the R1620L line. A The R1620L mutation is located in the S4 segment of the DIV transmembrane domain. **B** Gel electrophoresis image of the digested PCR product (left), confirmed by Sanger sequencing (right). *Taq* 1 digestion of the PCR product yielded two fragments (610 and 176 bp) from the mutant allele, while the WT allele was identified by the uncut 786 bp PCR product (Fig. 1B). **C** Homozygous mutants die by postnatal day 22 (P22). Approximately 20% of heterozygous mutants die by P60. **D** $Na_v1.6$ protein levels were not significantly different between WT littermates, RL/+ mutants, and RL/RL mutants; Kruskal–Wallis test followed by Dunn's multiple comparisons test. Data are presented as normalized to WT levels with the average WT density = 1. $N = 5$–7/genotype. Data are presented as mean ± SEM.

with autism or intellectual disability, the de novo heterozygous *SCN8A* R1620L mutation was found in an individual who presented with a range of behavioral abnormalities, including autism, attention deficit hyperactivity disorder, dyskinesia, aggression, and social behavior deficits [20, 21]. Behavioral seizures without accompanying electrographic seizure activity were also noted [21]. To date, the R1620L mutation has only been found in one patient [20, 21]. We used CRISPR/Cas9 technology to introduce the R1620L mutation into the mouse *Scn8a* gene. We observed alterations in behavior, including hyperactivity, impaired learning and memory, and social behavior deficits. We also observed increased seizure susceptibility and spontaneous seizures in RL/+ mutants. Furthermore, we observed reduced neuronal firing frequency yet increased neuronal firing amplitude in the RL/+ mutants. Finally, we demonstrated that oxcarbazepine and Huperzine A were capable of conferring robust seizure protection. Compared to the *Scn8a*$^{N1768D/+}$ and conditional R1872W mutants (expressed globally or in excitatory neurons), RL/+ mutants exhibit a normal lifespan, a wide range of behavioral abnormalities, and increased seizure susceptibility, thus providing insight into the broad spectrum of phenotypes associated with *SCN8A* dysfunction and opportunities for therapy development.

MATERIALS AND METHODS

Animals

Using CRISPR/Cas9 technology, we introduced the human R1620L mutation into the equivalent location of the mouse *Scn8a* gene (R1618 in the mouse) on the C57BL/6J background (Fig. 1A, Supplementary Fig. 1A). Cas9 protein was used for the mutagenesis since it has been shown to initiate editing in embryos more rapidly than Cas9 mRNA. Furthermore, Cas9 protein provides high editing efficiency, lower off-target effects, and reduced mosaicism compared to Cas9 mRNA [22, 23]. Two silent substitutions were also introduced in order to create a *Taq 1* restriction enzyme site. *Taq* 1 digestion of the PCR product yielded two fragments (610 and 176 bp) from the mutant allele, while the wild-type (WT) allele was identified by the uncut 786 bp PCR product (Fig. 1B). Heterozygous mice (RL/+) were backcrossed to C57BL/6J mice (Strain: 000664, Jackson Laboratories) for four generations to eliminate off-target substitutions. To identify possible off-target substitutions, whole-genome sequencing was performed on 2 RL/+ mutants and 1 WT littermate at the N4 generation (PerkinElmer Genomics). Sequence data from all chromosomes were examined for coding variants that differed between the mutant and WT mice. The only observed nucleotide change that resulted in an amino acid substitution in the RL/+ mutants but not the WT littermates corresponded to the engineered mutation in *Scn8a*. We also performed Sanger sequencing of all *Scn8a* exons in a RL/+ mutant and confirmed the absence of unwanted substitutions. All mice were housed on a 12-h light/dark cycle with food and water available ad libitum. All experiments were performed in accordance with the guidelines of the Institutional Animal Care and Use Committee of Emory University.

Behavioral assessment of RL/+mice

Behavioral analyses were conducted in male RL/+ mutants and WT littermates (3–4 months old, $N = 9$–10/genotype) as previously described [10, 24–27]. The same cohort of mice was used sequentially for all behavioral assessments, with one week to recover between behavioral tests. A separate cohort of mice ($N =$ 10/genotype) were used for pain analyses and nerve conduction velocity ($N = 5$–6/genotype). Behavior was assessed using several behavioral tasks with the most stressful task performed last: open field, novel object recognition, rotarod, three-chamber social interaction, light/dark box, novel cage, reciprocal interaction, and fear conditioning. All mice were transported to the behavior room

at 7 a.m. and allowed to acclimate for 2 h prior to testing. All behavior testing was performed and completed between 9 a.m. and 2 p.m.

Assessment of seizure susceptibility

Seizure susceptibility was evaluated using four seizure induction paradigms: 6 Hz, flurothyl, pentylenetetrazole (PTZ), and hyperthermia as previously described [24, 26–30]. Male and female RL/+ mutants and WT littermates (2–4 months old) were used for all seizure induction paradigms (except hyperthermia induction) and spontaneous seizure detection.

EEG analyses

One month of continuous EEG/video recording was obtained for each mouse, and EEG/EMG signals were collected and analyzed with Stellate Harmonie rodent EEG software [10, 24, 28]. A high-pass filter of 5 Hz, a low-pass filter of 70 Hz, and a notch filter of 60 Hz was used to analyze EEG/EMG signals. Seizures were characterized by high frequency and amplitude EEG signals that lasted for at least 3 s and were at least twice the background. The experimenter was blind to genotype when manually examining EEG traces and scoring seizure frequency and duration. Behavioral seizures were confirmed by simultaneous video recordings.

Assessment of electrophysiological properties

Electrophysiological recordings were obtained using a MultiClamp 700B amplifier (Molecular Devices, Union City, CA), digitized with a Digidata 1322A digitizer (Molecular Devices), and data were acquired and analyzed with pClamp 10.2 software (Molecular Devices). Cells were visualized using infrared DIC illumination under 40× magnification. Firing patterns were recorded in response to 2-s depolarizing current injections in 20-pA increments, from −30 to 130 pA. Firing properties, such as threshold, half-width, height, and latency, were measured for the first action potential (AP) fired during current clamp step protocol with increasing current injections (−10 to 130 pA).

Miniscope calcium imaging

In vivo GCaMP6f-based calcium imaging of population bV1 neurons was performed in awake, freely behaving male mice ($N = 3$/genotype; WT = 432 neurons, RL/+ = 420 neurons). Behavioral recordings were performed by tracking the location of the LED on the miniscope through the experimental sessions. Calcium imaging was recorded during 5 min of baseline behavior prior to PTZ administration (30 mg/kg, s.c., $N = 2$/genotype; WT = 289 neurons, RL/+ = 289 neurons); recordings continued for 15 min after PTZ.

Additional "Materials and methods" can be found in the Supplementary Materials and methods.

STATISTICS

Data in this study are expressed as mean ± SEM with $P \leq 0.05$ considered as statistically significant. All statistical analyses were performed with Prism 8.0 (GraphPad Software, San Diego, CA) and IBM SPSS version 26 (Armonk, NY). A description of the statistical analysis for each behavioral assessment, susceptibility to induced seizures, and electrophysiology can be found in Tables S1, S2, and S3, respectively. A Levene's test and Shapiro–Wilk test were used to determine the homogeneity of variance and normality for each task, respectively. A Chi-square test was used to compare the observed number of offspring of each genotype to the expected Mendelian ratio. A Kruskal–Wallis test was used to compare $Na_v1.6$ protein levels between homozygous RL/RL mutants, heterozygous RL/+ mutants, and WT littermates. An unpaired Student's t test was used to compare distance traveled, average speed, and time spent in the center of the apparatus between RL/+ mutants and WT littermates in the open field paradigm. An unpaired Student's t test was used to compare the discrimination ratio between RL/+ mutants and WT littermates in the novel object recognition paradigm. A two-way rANOVA was used to compare the latency to fall from the rotarod between RL/+ mutants and WT littermates. In the three-chamber paradigm, a two-way ANOVA was used to compare the time spent interacting with (1) the empty cage or stranger mouse and (2) a familiar and stranger mouse between RL/+ mutants and WT littermates. In the reciprocal interaction paradigm, a Mann–Whitney test was used to compare the latency to interact and time interacting between pairs of RL/+ mutants and WT littermates. An unpaired Student's t test was used to compare the total time spent in the lit side of the light/dark box between RL/+ mutants and WT littermates. In the novel cage paradigm, a Mann–Whitney test was used to compare the time spent sniffing, digging, grooming, and jumping between RL/+ mutants and WT littermates. A two-way rANOVA followed by Sidak's multiple comparisons test was used to compare percent freezing across the three trials on Day 1 between RL/+ mutants and WT littermates for the fear conditioning paradigm. A Mann–Whitney test was used to compare percent freezing on Day 2 and Day 3 between RL/+ mutants and WT littermates. An unpaired Student's t test was used to compare mechanical and thermal sensitivity, peripheral edema, and the effect of CFA on mechanical sensitivity between RL/+ mutants and WT littermates. A Kruskal–Wallis test was used to compare conduction velocity between homozygous RL/RL mutants, heterozygous RL/+ mutants, and WT littermates.

A Mann–Whitney test was used to compare Racine scores following 6 Hz-induced seizures between RL/+ mutants and WT littermates. A Mann–Whitney test was used to compare the time to recover from a 6 Hz-induced seizure in female RL/+ mutants and WT littermates. A Mann–Whitney test was used to compare the latency to the myoclonic jerk and generalized tonic–clonic seizure (GTCS) following flurothyl in male RL/+ mutants and WT littermates. An unpaired Student's t test was used to compare the latency to the myoclonic jerk and GTCS following flurothyl between female RL/+ mutants and WT littermates. An unpaired Student's t test and Mann–Whitney test were used to compare the latency to the MJ and GTCS following PTZ administration between female RL/+ mutants and WT littermates, respectively. A log-rank (Mantel–Cox) test was used to compare temperature curves between RL/+ mutants and WT littermates following hyperthermia induction. A Friedman's test was used to compare firing frequency between WT littermates and RL/+ mutants. A Mann–Whitney test was used to compare amplitude and intrinsic properties of CA3 hippocampal neurons between WT littermates and RL/+ mutants. A Mann–Whitney test was used to compare neuron firing frequency and amplitude of bV1 neurons between WT and RL/+ mutants. A Kruskal–Wallis test followed by Dunn's multiple comparisons test was used to compare the effect of OXC on 6 Hz-induced seizures in RL/+ mutants. A Friedman's test was used to compare Racine scores after Hup A treatment in RL/+ mutants and WT littermates. A log-rank (Mantel–Cox) test was used to compare the curves for the percentage of RL/+ mutants and WT littermates exhibiting a PTZ-induced GTCS after OXC or Hup A treatment. For all experiments, the experimenter was blind to genotype and treatment.

RESULTS

RL/+ mutants exhibit reduced lifespan

Male and female RL/+ mutants were crossed to generate homozygous RL/RL, heterozygous RL/+, and WT littermates. From a total of 15 litters, we observed WT (44), RL/+ (74), and RL/RL (33) offspring, which is consistent with the predicted 1:2:1 Mendelian ratio ($P = 0.44$). A tremor involving the forelimbs and hindlimbs was observed in the RL/RL mutants beginning around P15, which progressively worsened until they could no longer maintain an

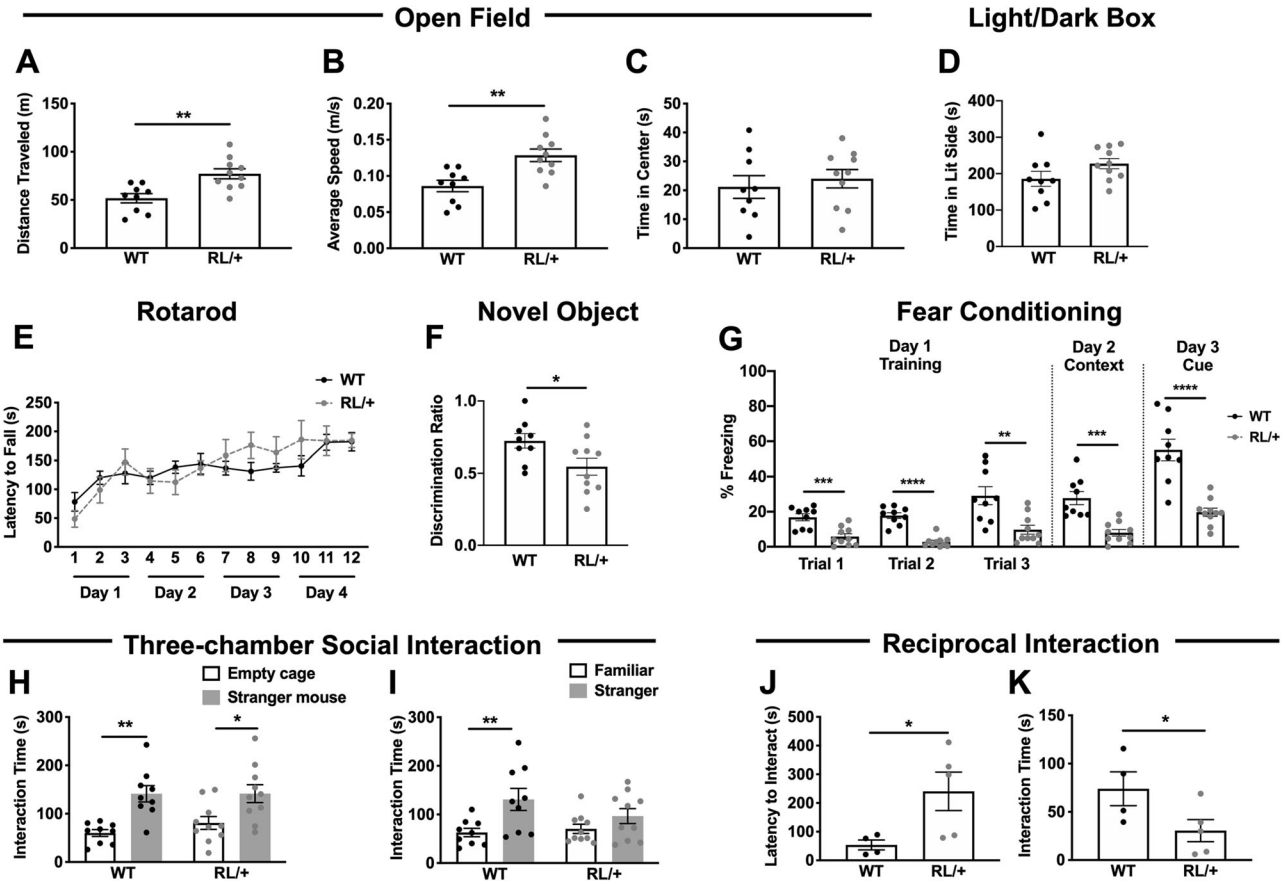

Fig. 2 RL/+ mutants exhibit abnormal behaviors. A, **B** RL/+ mutants traveled significantly farther and faster than WT littermates in the open field paradigm; unpaired student's *t* test. **C** RL/+ mutants and WT littermates spent similar lengths of time in the center of the open field; unpaired student's *t* test. **D** RL/+ mutants and WT littermates spent similar amounts of time in the lit side of the light/dark box; unpaired student's *t* test. **E** Motor learning is comparable between RL/+ mutants and WT littermates; two-way rANOVA. **F** RL/+ mutants exhibit impaired learning and memory in the novel object recognition paradigm; unpaired student's *t* test. **G** RL/+ mutants exhibit significantly less freezing behavior during the training (Day 1), context (Day 2), and cue (Day 3) sessions of the fear conditioning paradigm; two-way rANOVA followed by Sidak's multiple comparisons test and Mann–Whitney test. **A–G** $N = 9$–10/genotype. **H** RL/+ mutants and WT littermates spent more time exploring the stranger mouse than the empty cage. **I** WT littermates spent more time exploring the stranger vs. familiar mouse while RL/+ mutants spent similar lengths of time exploring the stranger and familiar mouse. **H**, **I**, $N = 9$–10/genotype; two-way ANOVA followed by Sidak's multiple comparisons test. **J** RL/+ mutants exhibit a significantly longer latency to interact and **K** interact significantly less compared to WT littermates in the reciprocal interaction paradigm. **J**, **K**, $N = 4$–5 pairs/genotype; Mann–Whitney test. $^{*}P \le 0.05$, $^{**}P \le 0.01$, $^{**}P \le 0.001$, $^{****}P \le 0.0001$. Data are presented as mean ± SEM.

upright position (P19–20). Weight gain was normal until P15, after which RL/RL mutants began to lose weight regardless of sex (Fig. S1B, C) and a maximum lifespan of 22 days was observed (Fig. 1C). EEG analyses in 2 RL/RL mutants (P19) confirmed that the observed shaking behavior was not associated with abnormal electrographic activity (Supplemental Video 1). It is possible the RL/RL mutants exhibit early mortality due to reduced muscle tone which would affect mobility, feeding behavior, or respiration. The mechanism underlying early death in the RL/RL mutants is therefore likely to be distinct from the factors that lead to SUDEP.

Normal $Na_v1.6$ protein levels in RL/+ mutant mice

Brains were extracted from WT, RL/+, and RL/RL mice (P21–22), and protein was isolated for western blot analysis. Comparable levels of $Na_v1.6$ were observed for all genotypes (Fig. 1D and Fig. S2), demonstrating that the R1620L mutation does not significantly alter protein levels.

RL/+ mutants are hyperactive

Since the proband with the *SCN8A* R1620L mutation was reported to exhibit a range of behavioral abnormalities [20, 21], we conducted a comprehensive behavioral comparison of male RL/+ mutants and WT littermates. In the open field paradigm, RL/+ mutants traveled significantly farther and faster than WT littermates (Fig. 2A, B, $P \le 0.01$), suggesting that the mutants are hyperactive. The time spent in the center of the open field was not significantly different between RL/+ mutants and WT littermates, suggesting a normal level of anxiety (Fig. 2C).

RL/+ mutants exhibit normal anxiety levels

Anxiety-like behavior was also evaluated using the light/dark box. Consistent with our measure of time spent in the center of the open field apparatus, there were no significant differences between the WT littermates and RL/+ mutants in the time spent in the lit side of the light/dark box, demonstrating normal anxiety levels (Fig. 2D, Table S1).

In the novel cage paradigm, we found that the RL/+ mutants and WT littermates spent comparable lengths of time grooming, digging, and sniffing (Fig. S3A–C). Although not statistically significant, we did observe repetitive jumping behavior in 40% (4 of 10) of RL/+ mutants (Fig. S3D). This behavior was characterized by the mutant mice jumping up and down in the same spot for periods of 15–30 s. This behavior was absent in the WT littermates.

RL/+ mutants display normal motor learning
We evaluated motor learning and coordination using an accelerating rotarod. RL/+ mutants and WT littermates exhibited comparable motor coordination and motor learning (Fig. 2E). We also examined nerve conduction velocity (P14–15) as previous studies reported reduced nerve conduction velocity in some mice expressing mutant *Scn8a* alleles [27, 31, 32]. No difference in nerve conduction velocity was observed across genotypes (Fig. S4).

RL/+ mutants exhibit impaired learning and memory
In the novel object recognition paradigm, as expected, the WT littermates spent significantly more time exploring the novel object compared to the familiar object (Fig. 2F). However, the RL/+ mutants failed to discriminate between the novel and familiar objects, suggesting a deficit in long-term learning and memory (Fig. 2F). We used the fear conditioning paradigm to evaluate associative learning and memory [25]. On Day 1, the WT littermates spent significantly more time freezing after each exposure to the tone compared to the RL/+ mutants. During both the context (Day 2) and cue trials (Day 3), the RL/+ mutants exhibited significantly less freezing behavior compared to the WT littermates (Fig. 2G), suggesting impaired associative learning and memory. However, this result should be interpreted with caution as the RL/+ mutants and WT littermates did not display comparable freezing behavior during the training sessions (Fig. 2G).

RL/+ mutants and WT littermates have comparable mechanical and thermal sensitivities
No significant differences in mechanical threshold and thermal sensitivity between RL/+ mutants and WT littermates ($N = 10$/genotype) were observed (Table S1). Furthermore, following injection of complete Freund's adjuvant (CFA), mechanical sensitivity (von Frey) and paw diameter (swelling of the paw after CFA) were not significantly different between genotypes (Table S1). These findings indicate that peripheral and central pain responses are comparable between RL/+ mutants and WT littermates.

RL/+ mutants may have impaired social behavior
Social behavior was compared between RL/+ mutants and WT littermates using the three-chamber social interaction paradigm and the reciprocal interaction task. In the three-chamber social interaction paradigm, there were no significant differences in the time exploring the empty cage vs. stranger mouse between WT littermates and RL/+ mutants (Table S1). Both the WT littermates ($P \leq 0.01$) and RL/+ mutants ($P \leq 0.05$) spent significantly more time interacting with the stranger mouse compared to the empty wire cage, demonstrating normal sociability (Fig. 2H). As a measure of social discrimination, the time spent exploring a familiar vs. stranger mouse was compared (Table S1). No significant difference in exploration times was observed between WT littermates and RL/+ mutants (Fig. 2I). However, while WT littermates spent significantly more time interacting with the stranger mouse compared to the familiar mouse ($P \leq 0.01$), the RL/+ mutants spent similar lengths of time ($P = 0.37$). It is possible that the learning and memory deficits identified in the RL/+ mutants, based on performance in the novel object recognition paradigm, could have influenced the ability of the RL/+ mutants to learn and remember the familiar mouse and therefore may have confounded their ability to discriminate between a familiar and stranger mouse.

To further examine whether the RL/+ mutants have an impairment in social behavior, we performed the reciprocal interaction task. In this paradigm, pairs of stranger mice of the same genotype were placed in a novel mouse cage and observed for 10 min. RL/+ mutants exhibited a greater latency to interact (Fig. 2J), and spent less time interacting compared to WT littermates (Fig. 2K). Both of these differences were statistically significant ($P \leq 0.05$), suggesting the RL/+ mutants may have an impairment in social interaction. Fighting was not observed.

RL/+ mutants exhibit increased susceptibility to induced seizures
We first compared susceptibility to 6 Hz-induced seizures between RL/+ mutants and WT littermates at a current intensity of 16 mA. Seizures occurred in all male RL/+ mutants, while seizures were not observed in the male WT littermates (Fig. 3A, $P \leq 0.0001$). Seizures were similarly observed in all female RL/+ mutants and 5/11 female WT littermates (Fig. 3B, $P \leq 0.01$). To determine whether we could achieve more separation between female RL/+ mutants and WT littermates, we repeated the 6 Hz paradigm at a lower current (14 mA) in a separate cohort of female mice (Fig. 3C, $P \leq 0.0001$). All female RL/+ mutants exhibited a seizure at the lower current, while most of the female WT littermates did not seize. We also found that female RL/+ mutants took longer to recover from a 6 Hz-induced seizure compared to the WT littermates that seized (Fig. 3D, $P \leq 0.05$, $N = 18$/genotype). Recovery time was not determined for male mice since seizures were not observed in male WT littermates.

We next evaluated susceptibility to the chemoconvulsant flurothyl. Regardless of sex, we observed a reduced latency to the first myoclonic jerk (MJ) and GTCS in RL/+ mutants compared to WT littermates (Fig. 3E–H). Consistent with the flurothyl results, we also observed increased susceptibility to PTZ in RL/+ mutants compared to WT littermates (Fig. S5).

Finally, we evaluated susceptibility to hyperthermia-induced seizures in two cohorts of mice: Cohort 1: RL/RL mutants, RL/+ mutants, and WT littermates (P13–14) and Cohort 2: RL/+ mutants and WT littermates (P21–23). As core body temperature was raised, myoclonic jerks were observed in all RL/+ mutants from both Cohorts and all RL/RL mutants in Cohort 1, but not in the WT littermates. In Cohort 1, 14/17 RL/+ mutants and 8/8 RL/RL mutants exhibited a GTCS. The average temperature at GTCS onset was significantly lower in RL/RL mutants compared to RL/+ mutants ($P \leq 0.0001$) and compared to 42.5 °C (maximum temperature of the WT littermates, Fig. 3I, $P \leq 0.001$). In Cohort 2, 5 of 7 RL/+ mutants exhibited a GTCS (Fig. 3J, $P \leq 0.01$). None of the WT littermates in either cohort exhibited a GTCS following hyperthermia induction.

RL/+ mutants have spontaneous seizures
One month of continuous video/EEG recordings were obtained from RL/+ mutants ($N = 10$) and WT littermates ($N = 3$). Interictal spiking was only observed in the RL/+ mutants (Fig. S6A). Furthermore, spontaneous seizures were observed in 6/7 male RL/+ mutants and 2/3 female RL/+ mutants, with the total number of seizures ranging from 1–66 seizures/mouse during the recording period (Fig. S6B, C). No seizures were observed in the three WT littermates.

Pyramidal neurons in the hippocampal CA3 region of RL/+ mutants exhibit decreased firing frequency but a lower firing threshold
We compared the firing properties of CA3 pyramidal neurons from RL/+ and WT mice at current injections from −10 to 130 pA. Figure 4A shows an example of intrinsic firing by WT and RL/+ CA3 pyramidal neurons injected with 10 and 70 pA current. In pyramidal neurons from WT mice, the maximum average frequency was ~26 Hz (Fig. 4A, B). Compared to WT littermates, RL/+ neurons fired significantly fewer action potentials (APs) at all current injections, reaching a maximum average frequency of ~12 Hz (Fig. 4B, $Z = -6.939$, $P \leq 0.0001$). Although the maximum number of APs was reduced, the threshold for firing the first AP was significantly lower in pyramidal neurons from RL/+ mutants compared to WT littermates (Table S4, $P \leq 0.05$). This reduction in firing threshold is predicted to increase neural excitability. In

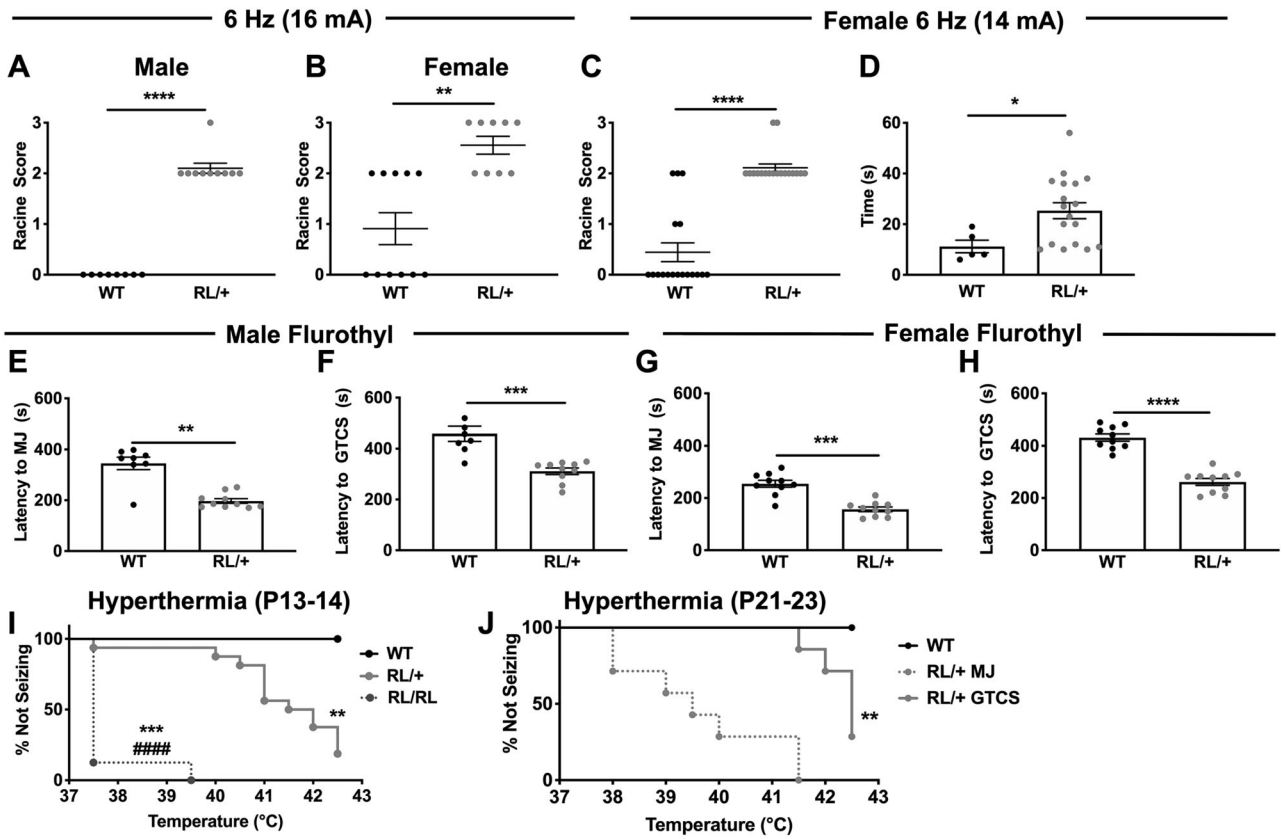

Fig. 3 RL/+ mutants exhibit greater susceptibility to induced seizures. Male (**A**) and female (**B**) RL/+ mutants are significantly more susceptible to 6 Hz-induced seizures compared to WT littermates (16 mA). **A**, **B** $N = 8–11$/genotype/sex; Mann–Whitney test. **C** Greater separation between female RL/+ mutants and WT littermates was observed at 14 mA. **D** Female RL/+ mutants take a significantly longer time to recover following a 6 Hz-induced seizure compared to WT littermates, **C**, **D** $N = 18$/genotype; Mann–Whitney test**.** **E** Male RL/+ mutants exhibit a significantly shorter latency to the first myoclonic jerk (MJ) and **F** generalized-tonic–clonic seizure (GTCS) compared to WT littermates. **E**, **F** $N = 8–10$/genotype; Mann–Whitney test. **G** Female RL/+ mutants exhibit a significantly shorter latency to the first MJ and **H** GTCS compared to WT littermates. **G**, **H** $N = 10$/genotype; unpaired student's *t* test. **I** All P13-P14 homozygous RL/RL mutants (8/8) exhibited a GTCS, compared to 14/17 (82%) of RL/+ mutants and 0/6 WT littermates. GTCS generation also occurred at lower average temperatures in RL/RL compared to RL/+ mutants. $N = 6–17$/genotype. *compared to WT, #compared to RL/+ ; log-rank (Mantel–Cox) test. **J** In an older cohort of mice (P21–P23), all heterozygous RL/+ mutants exhibited a MJ, and 5/7 (71%) of these mutants had a GTCS. WT littermates were taken to the maximum temperature (42.5 °C) but did not exhibit either a MJ or GTCS. $N = 7–8$/genotype. *compared to WT; log-rank (Mantel–Cox) test. *$P \leq 0.05$, **$P \leq 0.01$, ***$P \leq 0.001$, ****$P \leq 0.0001$. Data are presented as mean ± SEM.

addition, the AP half-width was significantly higher in RL/+ neurons compared to WT neurons (Table S4, $P \leq 0.001$), which suggests that the neurons would spend more time in a depolarized state, consistent with increased excitability.

Calcium imaging reveals reduced firing frequency but increased firing amplitude in excitatory neurons of RL/+ mutants

Extending hippocampal slice recordings to in vivo physiology, we performed Ca^{2+} imaging experiments in the visual cortex of freely moving animals (Fig. 4C, D). The visual cortex is routinely studied in epilepsy [33–35] and offers the advantage of imaging population neurons at single cell resolution below the brain surface without surgical damage. Furthermore, imaging of visual cortical responses is preferred as the cortex does not display the place specific activity that is known to occur in the hippocampus, thus facilitating data analysis [36]. At baseline, excitatory neurons in the visual cortex of RL/+ mutants exhibited significantly reduced firing frequency compared to WT littermates (Fig. 4G, $P \leq 0.001$). However, firing amplitudes were significantly larger in RL/+ mutants compared to WT littermates, suggesting increased neural excitability in the mutants (Fig. 4H, $P \leq 0.001$). Following low-dose PTZ administration (30 mg/kg), RL/+ mutants exhibited significantly increased neural firing frequency and amplitude compared to baseline (Fig. 4K, L, $P \leq 0.001$, Supplemental Video 2), whereas there were no differences in neural firing frequency and amplitude in WT littermates after PTZ administration. PTZ treatment in the RL/+ mutants elicited behavioral seizures which were not observed in the WT littermates.

Oxcarbazepine and Huperzine A protect against induced seizures in RL/+ mutants

Oxcarbazepine (OXC), a sodium channel blocker, has previously been used in patients with *SCN8A* epileptic encephalopathy [37]. We generated a dose–response curve using the 6 Hz seizure induction paradigm and found that OXC (10–50 mg/kg) was capable of increasing resistance against 6 Hz-induced seizures (Fig. 5A). We did not observe any adverse effects in the WT littermates at any of the OXC doses tested. Regardless of genotype, we found that OXC (50 mg/kg) significantly increased the latency to the first GTCS following PTZ administration (Fig. 5B). In addition, 5/9 OXC-treated WT littermates did not exhibit a GTCS; however, all RL/+ mutants regardless of treatment exhibited a GTCS (Fig. 5B).

We previously demonstrated that Huperzine A (Hup A) provided robust protection against induced seizures in *Scn1a* mouse models of Dravet syndrome and GEFS+ [29]. To establish whether Hup A could be similarly protective in *SCN8A*-derived epilepsy, we examined the effect of Hup A administration (1 mg/kg)

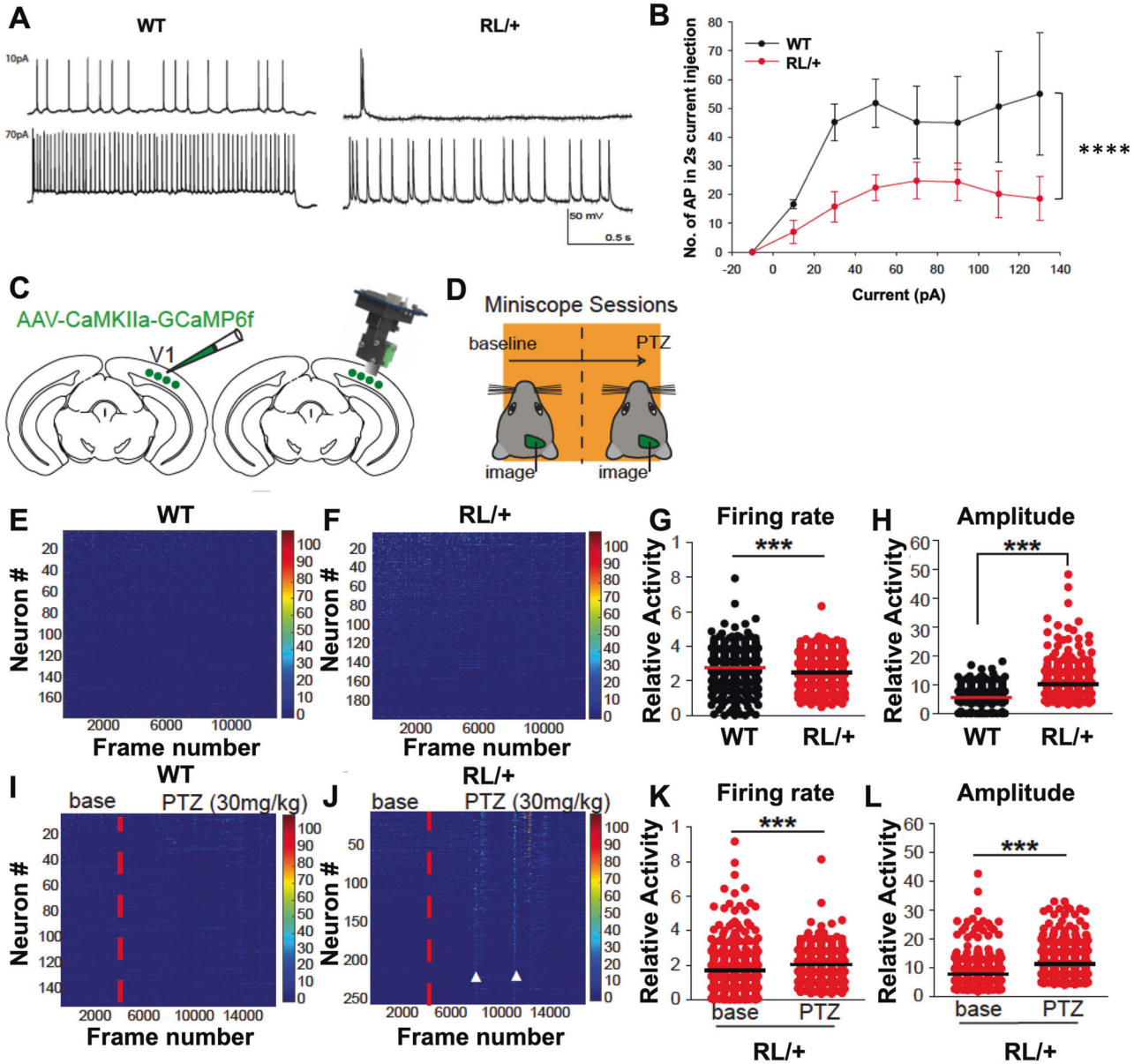

Fig. 4 RL/+ mutants exhibit significantly increased neural excitability and seizure susceptibility. A Representative action potential firing pattern in WT (left) and RL/+ (right) neurons observed during injection of 10 and 70 pA. **B** The number of action potentials fired during a 2-s current injection is plotted against the corresponding level of current. RL/+ mutants had significantly less firing compared to WT; Friedman's test. **C** Cartoon depicting viral injection (AAV-CAMK2a-GCaMP6f) into visual cortex and placement of GRIN lens at the injection site to allow for miniscope recordings. **D** Experimental timeline. Recordings were first conducted at baseline (data shown in **E–H**). One week later, mice were subjected to 5 min of baseline recordings followed by PTZ administration. Recordings continued for 15 min after PTZ (data shown in **I–L**). **E** Representative raster plot of neural calcium response of three WT littermates (432 total number of neurons), and **F** 3 RL/+ mutants (420 total number of neurons). **G** Distribution of single cell firing rates (WT: mean ± SD = 0.28 ± 0.11 Hz, RL/+ : mean ± SD = 0.25 ± 0.08 Hz). Firing rate is calculated by (total number of calcium peaks)/(total time); Mann–Whitney test. **H** Distribution of single cell sum peak amplitudes (WT: mean ± SD = 6.02 ± 3.26 dF/F, RL/+ : mean ± SD = 11.82 ± 5.35 dF/F); Mann–Whitney test. **I**, **J** Raster plots of neural calcium response from two WT (289 total number of neurons) and two RL/+ mice (289 total number of neurons) before and after PTZ administration (vertical red dotted line). **J** RL/+ mutants exhibited large synchronous neural responses during seizures (white arrow heads). **K** Distribution of single cell firing rates during baseline or PTZ sessions for RL/+ mutants. RL/+ baseline: mean ± SD = 0.16 ± 0.12 Hz, RL/+ PTZ: mean ± SD = 0.21 ± 0.0811 Hz. WT littermates did not show significantly increased firing rates after PTZ treatment; Mann-Whitney test. **L** Distribution of single cell sum peak amplitudes in baseline or PTZ sessions for RL/+ mice; RL/+ baseline: mean ± SD = 7.89 ± 5.10 Hz, RL/+ PTZ: mean ± SD = 11.15 ± 5.98 Hz. WT littermates did not exhibit significantly increased amplitudes after PTZ administration; Mann–Whitney test. ***$P \leq 0.001$, ****$P \leq 0.0001$. Data are presented as mean ± SD.

on susceptibility to 6 Hz- and PTZ-induced seizures in RL/+ mutants and WT littermates. All Hup A-treated RL/+ mutants were completely protected against 6 Hz-induced seizures, whereas all vehicle-treated RL/+ mutants seized (Fig. 5C, $P \leq 0.0001$). Hup A also significantly increased the latency to the first PTZ-induced GTCS in both the mutants and WT littermates (Fig. 5D). Interestingly, while all OXC-treated mutants exhibited a PTZ-induced GTCS, 5 of 8 Hup A-treated RL/+ mutants did not, suggesting that Hup A might provide more robust seizure protection.

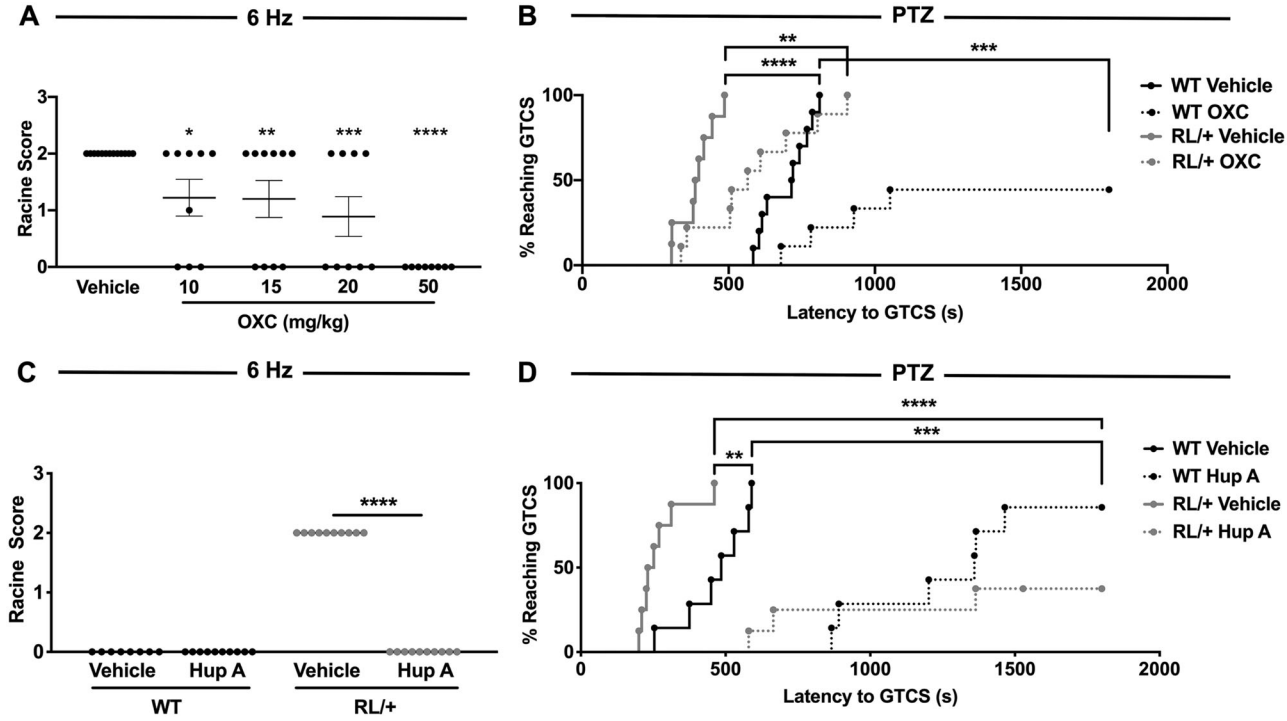

Fig. 5 Oxcarbazepine and Huperzine A increase resistance to 6 Hz- and PTZ-induced seizures in RL/+ mutants. A OXC significantly increases resistance to 6 Hz-induced seizures in the RL/+ mutants. $N = 9–13$/group; Kruskal–Wallis test followed by Dunn's multiple comparisons test. **B** OXC (50 mg/kg) significantly increases the latency to PTZ-induced GTCS in RL/+ mutants and WT littermates; however, the number of RL/+ mutants exhibiting a GTCS was comparable to vehicle-treated mutants. $N = 8–9$/group; log-rank (Mantel–Cox) test. **C** Hup A (1 mg/kg) confers robust protection against 6 Hz-induced seizures in RL/+ mutants. $N = 9–10$/group; Friedman's test. **D** Hup A (1 mg/kg) significantly increased the latency to PTZ-induced GTCS in RL/+ mutants and WT littermates and reduced the number of mutants and WT littermates that exhibited a GTCS. $N = 7–8$/group. $^{*}P \le 0.05$, $^{**}P \le 0.01$, $^{***}P \le 0.001$, $^{****}P \le 0.0001$. Data are presented as mean ± SEM.

DISCUSSION

SCN8A R1620L, located in the DIVS4, was identified as a de novo heterozygous mutation in an individual diagnosed with autism spectrum disorder, other behavioral abnormalities, and behavioral seizures without accompanying electrographic seizure activity [20, 21]. Patients with autism often have deficits in social behavior. In the mouse, the reciprocal interaction task and the three-chamber social interaction paradigm are used as measures of social behavior. Less interaction was observed between pairs of RL/+ mutants in the reciprocal interaction test, and the mutants did not show a preference for the stranger mouse during the social discrimination component of the three-chamber social interaction paradigm. These results suggest that social behavior may be impaired in the RL/+ mutants. Patients with autism may also exhibit other behavioral abnormalities, including hyperactivity, increased anxiety, and learning and memory deficits [38] which was congruent with our observations in the RL/+ mutants. The autistic-like behavioral characteristics observed in RL/+ mutants, and the similarity of these abnormalities to the clinical presentation of the R1620L patient [20, 21], indicate that RL/+ mutants are a good model to evaluate *SCN8A*-associated behavioral abnormalities (see Table S5 for a comparison of RL/+ mutants and other published *Scn8a* mouse models).

RL/+ mutants were found to exhibit significant impairment in long-term learning and memory, suggesting altered hippocampal function [39]. To evaluate whether other aspects of learning and memory are impaired in RL/+ mutants, we also attempted to examine associative learning using the fear conditioning paradigm. While the WT littermates showed the anticipated freezing response during the training period, RL/+ mutants unexpectedly exhibited significantly less freezing behavior (Fig. 2G). There are several potential explanations for the reduced freezing behavior in the RL/+ mutants. First, previous studies have demonstrated that lesions of the amygdala can result in a lack of freezing behavior in the fear conditioning paradigm [40, 41], raising the possibility that RL/+ mutants may have altered amygdala function. Second, it is conceivable that the reduced freezing behavior was due to the hyperactivity of the RL/+ mutants; however, hyperactivity has previously been observed in *Scn1a*$^{+/-}$ mutants that model Dravet syndrome, yet *Scn1a*$^{+/-}$ mutants displayed levels of freezing behavior comparable to their WT littermates during the training session of the fear conditioning paradigm [42]. Finally, it is possible RL/+ mutants have diminished sensitivity to the foot shock. In support of this, siRNA knockdown of $Na_v1.6$ has been shown to reduce pain-associated behaviors in a rat model of neuropathic pain [43]. However, our results demonstrated that RL/+ mutants have normal peripheral and central pain responses. To date, there is no reported sex difference in the clinical presentation of *SCN8A*-associated disease; however, it would be important to conduct behavioral analyses in female RL/+ mutants and WT littermates in future studies.

Patients with *SCN1A* mutations often exhibit febrile seizures (FSs) [44], which is modeled by the increased susceptibility of *Scn1a* mutants to hyperthermia-induced seizures [29, 30, 45, 46]. While patients with *SCN8A* mutations do not typically exhibit FSs, there have been some reports of FSs in these patients [37, 47–49]. Interestingly, RL/RL and RL/+ mutants exhibited increased susceptibility to hyperthermia-induced seizures compared to WT littermates. However, based on our observations, RL/+ mutants are less susceptible to hyperthermia-induced seizures compared to heterozygous *Scn1a* mutants [29, 30, 45], consistent with the less prominent role for FSs in *SCN8A*-associated disease.

Analyses of *SCN8A* mutations in heterologous systems have revealed varying effects of different mutations on hyperexcitability

[13, 21]. Two mutations found in patients with behavioral abnormalities but without severe epilepsy (A1622D and R1620L) exhibited in vitro alterations consistent with both gain- and loss-of-function effects. Compared to WT neurons, reduced peak current density, faster inactivation, and faster recovery from inactivation was observed when the R1620L mutation was expressed in rodent neuroblastoma ND7/23 cells [21]. We observed fewer APs during current injections into CA3 hippocampal pyramidal neurons from RL/+ mutants compared to WT littermates. We also found a significantly reduced threshold for firing the first AP and higher AP half-width in RL/+ mutant neurons, suggesting a combination of both potential gain- and loss-of-function effects of the mutation on neuronal excitability. It has been shown that impairments in CA3-induced network oscillations may contribute to autistic-like behaviors such as social interaction and memory deficits [50]. Therefore, it is possible that the reduced firing of CA3 pyramidal neurons in RL/+ mutants might contribute to some of the observed behavioral abnormalities.

To better understand neural circuit differences that underlie increased seizure susceptibility in the RL/+ mutants, we performed calcium imaging in freely behaving animals. At baseline, we observed decreased firing frequency and increased neuronal firing amplitude in visual cortex excitatory neurons in RL/+ mutants compared to WT littermates, again suggesting a combination of both gain- and loss-of-function effects. Furthermore, consistent with our observation of increased seizure susceptibility in the RL/+ mutants, PTZ increased both the amplitude and firing rate of bV1 neurons in the RL/+ mutants but not in WT mice.

The electrophysiological analyses and calcium imaging results demonstrate that the R1620L mutation exerts both gain- and loss-of-function effects on neuronal excitability. The gain-of-function property of this mutation is also supported by the observation that OXC, a sodium channel blocker, was able to increase seizure resistance in the RL/+ mutants. Interestingly, we found that Hup A, a reversible acetylcholinesterase inhibitor, conferred even greater protection against induced seizures in RL/+ mutants, raising the possibility that Hup A may also be beneficial in the treatment of *SCN8A* patients. Our observation of both gain- and loss-of-function effects of the R1620L mutation on neuronal excitability, and evidence of other *SCN8A* mutations with similar combinatorial effects [21], suggests an additional level of complexity likely underlies the mechanism by which some *SCN8A* mutations lead to disease. Given the recent advances in genetic therapies, these observations highlight the importance of mechanism-based therapeutic interventions for the treatment of channelopathies associated with epilepsy.

CONCLUSION

We generated a novel *Scn8a* mouse model by knocking-in the human R1620L mutation. RL/+ mutants exhibit a range of behavioral abnormalities, including hyperactivity, impaired learning and memory, social deficits, increased seizure susceptibility, and spontaneous seizures. Hippocampal CA3 pyramidal neurons from RL/+ mutants demonstrated both gain- and loss-of-function activity, which may account for the multiple phenotypic effects. Finally, we also demonstrated that OXC and Hup A confer robust protection against induced seizures in RL/+ mutants. This mouse line provides the opportunity to further evaluate the mechanistic basis for the range of clinical phenotypes associated with *SCN8A* mutations and for the development of new therapeutic approaches.

FUNDING AND DISCLOSURE

This project was supported in part by a postdoctoral fellowship from the American Epilepsy Society (JCW) and the National Institutes of Health (JCW, R21NS114795; GASI, F31NS110193; AE and ALG, R01NS090319; XX, R01NS104897). The content is solely the responsibility of the authors and does not necessarily reflect the official views of the National Institutes of Health. This project was also supported by the Rodent Behavioral Core, which is subsidized by the Emory University School of Medicine and is one of the Emory Integrated Core Facilities. Additional support was provided by the Emory Neuroscience NINDS Core Facilities (P30NS055077). Further support was provided by the Georgia Clinical & Translational Science Alliance of the National Institutes of Health under Award Number UL1TR002378. The authors have no financial interests relating to the work described and declare no competing interests.

ACKNOWLEDGEMENTS

The authors would like to acknowledge Dr. Mike Epstein for guidance on statistical analyses and Cheryl Strauss for editorial assistance.

AUTHOR CONTRIBUTIONS

JCW and AE designed the research studies and wrote the manuscript. JCW generated the mice with contribution from JTT. JCW performed the seizure and behavior experiments with contribution from JTT. SFG, LC, KD, XX, and ALG performed the slice electrophysiology and calcium imaging. GASI performed the Western blot analyses and nerve conduction velocity experiments. SP and SMG performed pain analysis. SFG, KD, GASI SMG, XX, and ALG contributed to editing the manuscript.

ADDITIONAL INFORMATION

Supplementary information The online version contains supplementary material available at https://doi.org/10.1038/s41386-021-00985-9.

Publisher's note Springer Nature remains neutral with regard to jurisdictional claims in published maps and institutional affiliations.

REFERENCES

1. Boiko T, Rasband MN, Levinson SR, Caldwell JH, Mandel G, Trimmer JS, et al. Compact myelin dictates the differential targeting of two sodium channel isoforms in the same axon. Neuron. 2001;30:91–104.
2. Boiko T, Van Wart A, Caldwell JH, Levinson SR, Trimmer JS, Matthews G. Functional specialization of the axon initial segment by isoform-specific sodium channel targeting. J Neurosci. 2003;23:2306–13.
3. Caldwell JH, Schaller KL, Lasher RS, Peles E, Levinson SR. Sodium channel Na(v)1.6 is localized at nodes of ranvier, dendrites, and synapses. Proc Natl Acad Sci USA. 2000;97:5616–20.
4. Hu W, Tian C, Li T, Yang M, Hou H, Shu Y. Distinct contributions of Na(v)1.6 and Na(v)1.2 in action potential initiation and backpropagation. Nat Neurosci. 2009;12:996–1002.
5. Raman IM, Sprunger LK, Meisler MH, Bean BP. Altered subthreshold sodium currents and disrupted firing patterns in Purkinje neurons of Scn8a mutant mice. Neuron. 1997;19:881–91.
6. Cummins TR, Dib-Hajj SD, Herzog RI, Waxman SG. Nav1.6 channels generate resurgent sodium currents in spinal sensory neurons. FEBS Lett. 2005;579:2166–70.
7. Hawkins NA, Martin MS, Frankel WN, Kearney JA, Escayg A. Neuronal voltage-gated ion channels are genetic modifiers of generalized epilepsy with febrile seizures plus. Neurobiol Dis. 2011;41:655–60.
8. Martin MS, Tang B, Papale LA, Yu FH, Catterall WA, Escayg A. The voltage-gated sodium channel Scn8a is a genetic modifier of severe myoclonic epilepsy of infancy. Hum Mol Genet. 2007;16:2892–9.
9. Makinson CD, Tanaka BS, Lamar T, Goldin AL, Escayg A. Role of the hippocampus in Nav1.6 (Scn8a) mediated seizure resistance. Neurobiol Dis. 2014;68:16–25.
10. Wong JC, Makinson CD, Lamar T, Cheng Q, Wingard JC, Terwilliger EF, et al. Selective targeting of Scn8a prevents seizure development in a mouse model of mesial temporal lobe epilepsy. Sci Rep. 2018;8:126.
11. Papale LA, Beyer B, Jones JM, Sharkey LM, Tufik S, Epstein M, et al. Heterozygous mutations of the voltage-gated sodium channel SCN8A are associated with spike-wave discharges and absence epilepsy in mice. Hum Mol Genet. 2009;18:1633–41.

12. Makinson CD, Tanaka BS, Sorokin JM, Wong JC, Christian CA, Goldin AL, et al. Regulation of thalamic and cortical network synchrony by Scn8a. Neuron. 2017;93:1165–79 e6.
13. Veeramah KR, O'Brien JE, Meisler MH, Cheng X, Dib-Hajj SD, Waxman SG, et al. De novo pathogenic SCN8A mutation identified by whole-genome sequencing of a family quartet affected by infantile epileptic encephalopathy and SUDEP. Am J Hum Genet. 2012;90:502–10.
14. Wagnon JL, Meisler MH. Recurrent and non-recurrent mutations of SCN8A in epileptic encephalopathy. Front Neurol. 2015;6:104.
15. Butler KM, da Silva C, Shafir Y, Weisfeld-Adams JD, Alexander JJ, Hegde M, et al. De novo and inherited SCN8A epilepsy mutations detected by gene panel analysis. Epilepsy Res. 2017;129:17–25.
16. Hammer MF, Wagnon JL, Mefford HC, Meisler MH, SCN8A-related epilepsy with encephalopathy, In: Adam MP, et al., editors. GeneReviews, Seattle, WA; 1993.
17. Wagnon JL, Korn MJ, Parent R, Tarpey TA, Jones JM, Hammer MF, et al. Convulsive seizures and SUDEP in a mouse model of SCN8A epileptic encephalopathy. Hum Mol Genet. 2015;24:506–15.
18. Bunton-Stasyshyn RKA, Wagnon JL, Wengert ER, Barker BS, Faulkner A, Wagley PK, et al., Prominent role of forebrain excitatory neurons in SCN8A encephalopathy. Brain. 2019;142:362–75.
19. Larsen J, Carvill GL, Gardella E, Kluger G, Schmiedel G, Barisic N, et al. The phenotypic spectrum of SCN8A encephalopathy. Neurology. 2015;84:480–9.
20. Rossi M, El-Khechen D, Black MH, Farwell Hagman KD, Tang S, Powis Z. Outcomes of diagnostic exome sequencing in patients with diagnosed or suspected autism spectrum disorders. Pediatr Neurol. 2017;70:34–43 e2.
21. Liu Y, Schubert J, Sonnenberg L, Helbig KL, Hoei-Hansen CE, Koko M, et al., Neuronal mechanisms of mutations in SCN8A causing epilepsy or intellectual disability. Brain. 2019.
22. Ma Y, Yu L, Pan S, Gao S, Chen W, Zhang X, et al. CRISPR/Cas9-mediated targeting of the Rosa26 locus produces Cre reporter rat strains for monitoring Cre-loxP-mediated lineage tracing. FEBS J. 2017;284:3262–77.
23. Yen ST, Zhang M, Deng JM, Usman SJ, Smith CN, Parker-Thornburg J, et al. Somatic mosaicism and allele complexity induced by CRISPR/Cas9 RNA injections in mouse zygotes. Dev Biol. 2014;393:3–9.
24. Lamar T, Vanoye CG, Calhoun J, Wong JC, Dutton SBB, Jorge BS, et al. SCN3A deficiency associated with increased seizure susceptibility. Neurobiol Dis. 2017;102:38–48.
25. Rha J, Jones SK, Fidler J, Banerjee A, Leung SW, Morris KJ, et al. The RNA-binding protein, ZC3H14, is required for proper poly(A) tail length control, expression of synaptic proteins, and brain function in mice. Hum Mol Genet. 2017;26:3663–81.
26. Wong JC, Shapiro L, Thelin JT, Heaton EC, Zaman RU, D'Souza MJ, et al. Nanoparticle encapsulated oxytocin increases resistance to induced seizures and restores social behavior in Scn1a-derived epilepsy. Neurobiol Dis. 2021;147:105147.
27. Inglis GAS, Wong JC, Butler KM, Thelin JT, Mistretta OC, Wu X, et al., Mutations in the Scn8a DIIS4 voltage sensor reveal new distinctions among hypomorphic and null Nav 1.6 sodium channels. Genes Brain Behav. 2019;19:e12612.
28. Shapiro L, Wong JC, Escayg A. Reduced cannabinoid 2 receptor activity increases susceptibility to induced seizures in mice. Epilepsia. 2019;60:2359–69.
29. Wong JC, Dutton SB, Collins SD, Schachter S, Escayg A. Huperzine A provides robust and sustained protection against induced seizures in Scn1a mutant mice. Front Pharmacol. 2016;7:357.
30. Wong JC, Thelin JT, Escayg A. Donepezil increases resistance to induced seizures in a mouse model of Dravet syndrome. Ann Clin Transl Neurol. 2019;6:1566–71.
31. Kearney JA, Buchner DA, De Haan G, Adamska M, Levin SI, Furay AR, et al. Molecular and pathological effects of a modifier gene on deficiency of the sodium channel Scn8a (Na(v)1.6). Hum Mol Genet. 2002;11:2765–75.
32. Angaut-Petit D, McArdle JJ, Mallart A, Bournaud R, Pincon-Raymond M, Rieger F. Electrophysiological and morphological studies of a motor nerve in 'motor endplate disease' of the mouse. Proc R Soc Lond B Biol Sci. 1982;215:117–25.
33. Hammad M, Schmidt SL, Zhang X, Bray R, Frohlich F, Ghashghaei HT. Transplantation of GABAergic interneurons into the neonatal primary visual cortex reduces absence seizures in stargazer mice. Cereb Cortex. 2015;25:2970–9.
34. Powell EM, Campbell DB, Stanwood GD, Davis C, Noebels JL, Levitt P. Genetic disruption of cortical interneuron development causes region- and GABA cell type-specific deficits, epilepsy, and behavioral dysfunction. J Neurosci. 2003;23:622–31.
35. Mainardi M, Pietrasanta M, Vannini E, Rossetto O, Caleo M. Tetanus neurotoxin-induced epilepsy in mouse visual cortex. Epilepsia. 2012;53:e132–6.
36. Sun Y, Jin S, Lin X, Chen L, Qiao X, Jiang L, et al. CA1-projecting subiculum neurons facilitate object-place learning. Nat Neurosci. 2019;22:1857–70.
37. Gardella E, Marini C, Trivisano M, Fitzgerald MP, Alber M, Howell KB, et al. The phenotype of SCN8A developmental and epileptic encephalopathy. Neurology. 2018;91:e1112–24.
38. Silverman JL, Yang M, Lord C, Crawley JN. Behavioural phenotyping assays for mouse models of autism. Nat Rev Neurosci. 2010;11:490–502.
39. Hammond RS, Tull LE, Stackman RW. On the delay-dependent involvement of the hippocampus in object recognition memory. Neurobiol Learn Mem. 2004;82:26–34.
40. Phillips RG, LeDoux JE. Differential contribution of amygdala and hippocampus to cued and contextual fear conditioning. Behav Neurosci. 1992;106:274–85.
41. Kim JJ, Rison RA, Fanselow MS. Effects of amygdala, hippocampus, and periaqueductal gray lesions on short- and long-term contextual fear. Behav Neurosci. 1993;107:1093–8.
42. Han S, Tai C, Westenbroek RE, Yu FH, Cheah CS, Potter GB, et al. Autistic-like behaviour in Scn1a+/- mice and rescue by enhanced GABA-mediated neurotransmission. Nature. 2012;489:385–90.
43. Xie W, Strong JA, Zhang JM. Local knockdown of the NaV1.6 sodium channel reduces pain behaviors, sensory neuron excitability, and sympathetic sprouting in rat models of neuropathic pain. Neuroscience. 2015;291:317–30.
44. Escayg A, Goldin AL. Sodium channel SCN1A and epilepsy: mutations and mechanisms. Epilepsia. 2010;51:1650–8.
45. Dutton SBB, Dutt K, Papale LA, Helmers S, Goldin AL, Escayg A. Early-life febrile seizures worsen adult phenotypes in Scn1a mutants. Exp Neurol. 2017;293:159–71.
46. Martin MS, Dutt K, Papale LA, Dube CM, Dutton SB, de Haan G, et al. Altered function of the SCN1A voltage-gated sodium channel leads to gamma-aminobutyric acid-ergic (GABAergic) interneuron abnormalities. J Biol Chem. 2010;285:9823–34.
47. Epifanio R, Zanotta N, Giorda R, Bardoni A, Zucca C. Novel epilepsy phenotype associated to a known SCN8A mutation. Seizure. 2019;67:15–17.
48. Encinas AC, Moore IKM, Watkins JC, Hammer MF. Influence of age at seizure onset on the acquisition of neurodevelopmental skills in an SCN8A cohort. Epilepsia. 2019;60:1711–20.
49. Zaman T, Abou Tayoun A, Goldberg EM. A single-center SCN8A-related epilepsy cohort: clinical, genetic, and physiologic characterization. Ann Clin Transl Neurol. 2019;6:1445–55.
50. Cellot G, Maggi L, Di Castro MA, Catalano M, Migliore R, Migliore M, et al. Premature changes in neuronal excitability account for hippocampal network impairment and autistic-like behavior in neonatal BTBR T+tf/J mice. Sci Rep. 2016;6:31696.